IOP Conf. Series: Journal of Physics: Conf. Series **1224** (2019) 012048 doi:10.1088/1742-6596/1224/1/012048

Experimental results on local heat transfer coefficient inside a rectangular channel with chevron-shaped ribs

P Gramazio, L Vitali, D Fustinoni, F Vignati and A Niro
Politecnico di Milano, Department of Energy,
Campus Bovisa, Via Lambruschini 4, 20156 Milano, Italy

Corresponding author email: alfonso.niro@polimi.it

Abstract. A non-intrusive measurement technique of the heat transfer coefficient field, based on IR-thermography, is applied on a 12-mm-height rectangular channel of 1:10 aspect ratio, whose lower surface is enhanced by chevron-shaped square-cross-section ribs. The channel is operated at imposed heat flux while forced-air flows for Reynolds numbers ranging from 700 to 8000. In particular, the technique uses local temperature measurements to retrieve the radiative heat flux with a three-wavelength-band model for partially transparent enclosures, and the conductive flux towards the backside with a FEM model, which allow an edge-to-edge estimation of the local convective heat transfer. The resulting local Nusselt number maps are presented and compared to data obtained operating both at fixed temperature and inside a channel with flat surfaces.

1 Introduction

A long-term scientific study on forced convection in channels in stationary conditions has been carried out by the ThermALab laboratory at Politecnico di Milano, focusing on the enhancing effect of ribs in several configurations on the convective heat transfer. In particular, a technique for the retrieval of the local Nusselt number has been first developed [1], then critically analyzed and corrected [2], and used after more considerations on its errors and critical aspects in a transverse ribs configuration [3].

In this work the focus is on V-shaped ribs, a configuration which is also called *chevron*. On this topic, starting from the 90s, studies have been carried out in order to enhance the effect of secondary flows, see for example Han et al. [4], Krukeja et al. [5], Gao and Sunden [6]. In general, V-shaped ribs may present the apex upwards or downwards with respect to the flow direction. In the former arrangement, secondary flows move from the centre to the lateral sides of the channel, whereas in the latter the situation is reversed. It has not been yet assessed which configuration is the best in enhancing heat transfer, because controversial results have been found, probably due to the different boundary conditions taken into consideration.

This paper shows the results of the adopted technique for the estimation of local convective heat transfer for a channel with V-shaped ribs on the bottom surface, which is heated with constant heat flux, for Reynolds numbers ranging from 700 to 8000, which encompasses the transitioning regime for the reference flat channel. In particular, the adopted technique allows the measurement near the edges of the channel, a region which is mostly overlooked by other works.

2 Materials and methods

2.1 Experimental apparatus

The measurements have been carried out on an open-loop channel operated in suction, as shown in figure 1. Summarizing its main features, the channel lower surface is heated by means of two Printed Circuit Boards (PCBs) independently powered and controlled. The PCBs have a substrate made of FR-4 fiberglass-reinforced epoxy laminate material, whereas copper tracks are 0.017 mm thick, 7.8 mm wide, spaced 0.2 mm apart each other, and covered by a black lacquer which also fills up the gaps between them, making the heating surface flat, smooth and with a high emissivity. A Hendress Hauser T-Mass 65F15 flow meter is used for automatic mass-flow rate readings. A double-glazing 130 mm x 130 mm germanium window grants the optical access to a FLIR T650sc IR-camera, with a 640 x 480-pixel resolution. The main experimental features are listed in table 1.

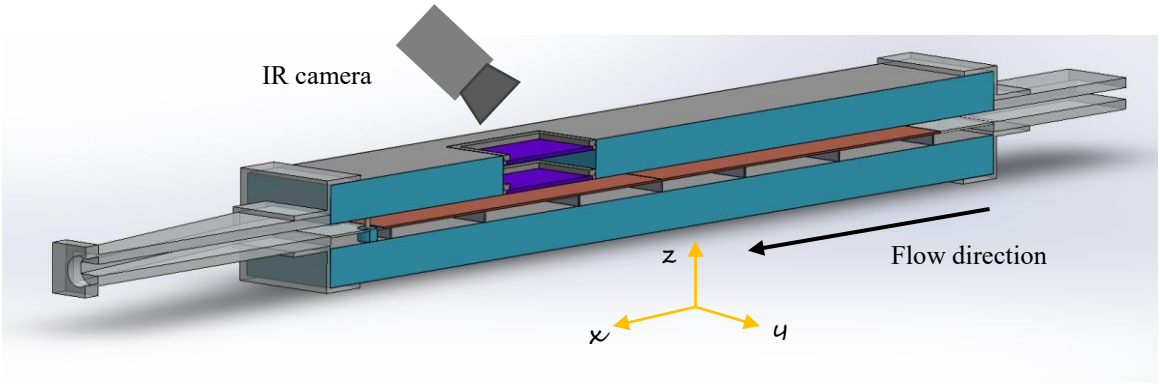

Figure 1. Section of the test channel for local heat transfer measurements, with constant heat flux

Table 1. Main experimental features

h	Channel height	12	mm
L	Channel length	840	mm
w	Channel width	120	mm
D_h	Hydraulic diameter	21.82	mm
	Height to width ratio	0.10	
s	Rib side dimension	4	mm
d	Distance rib-to-rib	80	mm
Re	Reynolds number	700 ≒ 8000	

Punctual temperature measurements are also carried out for reference by RTDs and thermocouples, as reported in table 2. The remaining temperatures, whose knowledge is needed to determine the convective heat flux distribution, are evaluated on the basis of the following assumptions, summarized in table 2 as well. The air bulk temperature $T_b(x)$ is assumed to have a linear increase along the test section, from the inlet value to the outlet one, as supposed by reference works [7]: while certainly an unrealistic assumption, as the air temperature is expected to vary in spanwise direction due to the rib configuration, since the procedure for retrieving the heat fluxes is already complex, the authors have opted for a simpler reference temperature to compute the local *h*, and therefore Nu.

The temperature of the germanium window $T_{ger}(x,y)$ is uniform and equal to the temperature T_{up} measured on its frame, as its conductivity is two orders of magnitude higher than all the other parts of the channel. Finally, the channel side wall temperature $T_{side}(x,z)$ is assumed to be constant along z-

direction and equal to the mean between T_{up} and the breadboard temperature T_{down} measured at the channel side.

Table 2. Main measured and derived temperature values

Measured Temperature	**Symbol**	**Probe kind/Instrument**
Bottom wall surface	$T_w(x,y)$	IR camera
External (ambient)	T_{ext}	PT100 RTD
Inlet air bulk temperature	T_{in}	PT100 RTD
Outlet air bulk temperature	T_{out}	PT100 RTD
Channel upper side wall	T_{up}	T-type thermocouple
Derived Temperature	**Symbol**	**Method**
Air bulk temperature	$T_b(x)$	Linear interpolation between T_{in} and T_{out}
Channel side wall	$T_{side}(x,z)$	Mean between T_{up} and $T_w(x,w/2)$
Germanium window surface	$T_{ger}(x,y)$	Uniform and equal to T_{up}

2.2 Modeling

The local convective heat transfer coefficient $h_{loc,q}$ and the related Nusselt number $Nu_{loc,q}$ are evaluated, for the channel with constant heat flux, as in equations 1 and 2:

$$h_{loc,q}(x,y) = \frac{q_c''(x,y)}{T_w(x,y) - T_b(x)} \tag{1}$$

$$Nu_{loc,q}(x,y) = \frac{h_{loc}(x,y)D_h}{k_{air}} \tag{2}$$

where $q''_c(x,y)$ and $T_w(x,y)$ are the punctual values of convective heat flux and surface temperature, respectively, and $T_b(x)$ is the air bulk temperature. Since the temperatures are known, the only term which requires a further specification is $q_c(x,y)$, and it is obtained by a steady-state balance on the copper track layer

$$q_c''(x,y) = \sigma_{el} s_{Cu} - q_r''(x,y) - q_{kz}''(x,y) + q_{kxy}''(x,y) \tag{3}$$

where σ_{el} the volumetric heat dissipation due to the Joule effect, considering a uniform generation, s_{cu} the layer thickness, $q''_r(x,y)$ the heat flux radiated by the layer coating, $q''_{kz}(x,y)$ the heat flux diffusing in z direction from the rear of the copper track layer toward the substrate inside, and finally $q''_{kxy}(x,y)$ the heat flux diffusing in x-y direction through the layer itself. This flux is considered negligible in streamwise x direction, i.e. parallel to the copper tracks, due to the small values of temperature gradient in that direction; in spanwise y direction, it is calculated for each $\bar{x}$, as

$$q_{kxy}''(\bar{x},y) = k_{eq} s_{Cu} \left(\frac{\partial^2 T_w}{\partial y^2} \right) \tag{4}$$

where k_{eq} the equivalent thermal conductivity, resulting from the series of the copper tracks and the lacquer filling the gaps between them. $q''_{kz}(x,y)$ and $q''_r(x,y)$ are calculated by means of a FEM model of the section and of a custom radiative model, respectively. The solution strategy is to apply those models on N_x independent 2D y-z slices of the test section, instead of solving two 3D problems, in order to reduce computational times and complexity without losing accuracy, as discussed in [1].

The adopted radiative model is the net radiation method for diffuse and gray surfaces, which has been modified by Siegel [8] to take into account semi-transparent surfaces. In particular, the method

allows to compute the radiative heat fluxes for each isothermal surface in enclosures with known temperature. In our case, the system is solved for each 2D section at fixed $\bar{x}$, by discretizing the PCB surface with Npixel elements, i.e. each pixel of the IR image is considered to be an isothermal surface. The lateral (XPS wall) and top (Germanium) surfaces, even if considered at uniform temperature, are discretized too, to increase the accuracy of the view factors computed by means of Hottel's method. Finally, the model is solved for three wavelength regions, i.e., between 0 and 7 μm, 7 and 13 μm, and from 13 μm up, which are determined by the selective transmittance behaviour of the germanium window. The total transmittance of the double-glazing has been taken into account for the top surface.

The main new aspect in the present work, with respect to the previous ones, is the unavoidable presence of the ribs in the 2D slices. Within the framework of this article, the authors have followed a "ribless" approach, thus the possible fin- or insulating-effect induced by the ribs and its consequences on the temperature field has been neglected and the rib-covered regions of the thermograms are just removed from the analysis.

2.3 Analysis procedure

The analysis procedure follows the steps described below:

- Start of the experimental setup, wait for stationary conditions;
- Acquisition of a sequence of thermograms and data from temperature sensors;
- Thermogram elaboration: time-average, projective transform, cut, slicing for analysis, 2D interpolation;

Then, for each slice:

- $q''_{kz}(x,y)$: inverse conductive FEM thermal problem, given the measured temperature field inside the channel and imposing natural convection and radiation b.c. towards the external environment (see figure 2)
- $q''_{ky}(x,y)$: second derivative of the temperature field
- $q''_{r}(x,y)$: 3-band radiative model for the channel cavity
- $q''_{c}(x,y)$: Application of equation 3

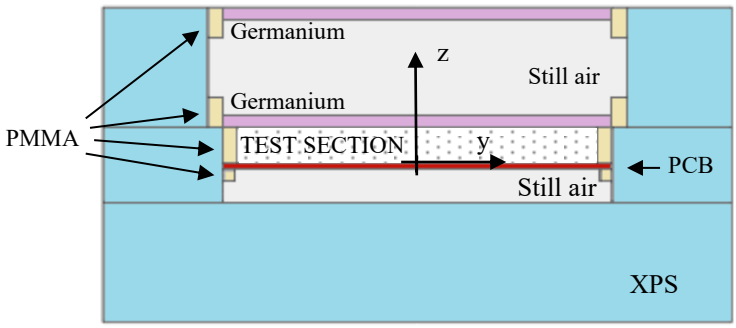

Figure 2. Geometry of the 2D FEM model of conductive heat transfer in the channel cross-section

3 Results

The local results show interesting trends. The whole spatial distribution of $Nu_{loc,q}(x,y)$ is depicted in figure 3, for three different values of Re. The selection of the three values of Re is made so that each Re would represent laminar, post-transitional and fully turbulent flow conditions in a corresponding smooth duct, respectively. It is known to Authors that the presence of the ribs affects the flow features,

so that the laminar-turbulent flow transition actually occurs at much lower Reynolds numbers, but the choice of the described operational conditions allows to directly compare the performances of the ribbed channel versus the smooth duct ones. Therefore, figures 3a, 3b and 3c concern cases tested at the minimum Re, i.e., Re=700, at an intermediate value, i.e., Re=5400, and at the largest Reynolds number, i.e., Re=7550. At Re=700, the onset of relevant secondary flows is evident, due to the presence of the ribs, which affect the near-wall flow and induce a non-zero spanwise velocity. The improved-mixing effect is relevant also on the heat transfer enhancement, as $Nu_{loc,q}(x,y)$ presents a significant trend in the spanwise direction, ranging approximately from 6 to 40. Also, the amplification of the local Nusselt number in the spanwise direction follows a 3.5:1 ratio, confirming the enhancement of the heat transfer coefficient due to the flow mixing. Similarly, also for larger Re values the improved mixing due to the ribs points to an increasing of the $Nu_{loc,q}(x,y)$ value from the centerline to lateral walls, which can be estimated around 3.5-4. Two additional considerations stem from the observation of figure 3: on the first hand, the geometrical symmetry of V-shaped ribs with respect to the centerline reflects on the flow features, and hence on the local Nusselt number, which is not spanwise-uniform, but still symmetrical, too. Moreover, by comparing the three maps, figures 3b and 3c appear to be much more similar to each other than figure 3a, pointing to a possible ceiling in the maximum effect of the flow mixing on heat transfer enhancement. This effect can be further observed in figure 6, as the average rib-to-rib Nu trend decreases its slope with the increase of Re.

From the full, two dimensional distributions of $Nu_{loc,q}(x,y)$, two plots are extracted, which allow to perform a one-dimensional but more accurate analysis. Figure 4 shows the spanwise distribution of $Nu_{loc,q}(x,y)$sampled at x=40mm in the streamwise direction, so that the spanwise measurements can be carried out along the whole channel amplitude, without interruptions due to the intersection between the sampling line and the ribs. All the three cases over different Re values are represented in the same picture, to better highlight similarities and differences due to the variation in the mass flow rate (and hence on the bulk velocity and Re). Moreover, the spanwise distribution of the Nusselt number as resulting from the study of the smooth channel is added (computed in the same Re), to assess the effect of the ribs as well. The first consideration concerns the different effects on heat transfer enhancement of the ribs versus Re. The variation induced by the Reynolds number on the local Nu when the ribs are absent is way lower than the corresponding one due to the introduction of the ribs: in the smooth channel, indeed, Nu is increased by an approximate factor of 3 when passing from Re=700 to Re=7550, whereas the point-wise improvement is by a factor of approximately 5 or 6 thanks to the introduction of the ribs. A fortunate side-consideration stems from figure 4, too, concerning the quality of the curves, which confirms the ability of the model to retrieve good results near the edges.

The second one-dimensional plot that can be extracted from the full $Nu_{loc,q}(x,y)$ map is depicted in figure 5, which shows the streamwise Nusselt trend. Both pictures 5a and 5b, representing Nu(x) sampled at the centerline and at 25% spanwise, respectively, show the same Nusselt streamwise distribution, regardless of the sampling position and of Re. As expected, Nu presents a periodic trend between couples of ribs. The shape of the axial distribution depends on whether Re is considered "large" (turbulent, with reference to the ribless channel) or "small" (laminar, with the same reference case). In the first case, for both Re=5400 and Re=7550, a pseudo-skewsymmetric trend of Nu(x) can be observed. At the rib trailing edge, at the beginning of the sampling range, Nu(x) presents an intermediate value, and it grows until it reaches the peak value, which is achieved at approximately 25% of the ribs pitch. Downstream the peak, Nu(x) decreases monotonously, and it approaches the initial value at approximately 50% of the ribs pitch. In the second half of the sampling range, Nusselt duplicates the first half trend but with an opposite fashion, as it decreases until the bottom value at approximately 75% of the ribs pitch, and then it restarts growing monotonously till the leading edge of the downstream rib. In this position, Nu is close but slightly lower than at trailing edge of the upstream rib. Conversely, at low Re (Re=700), the Nusselt distribution is quasi-uniform, presenting only a low, negligible inflation in correspondence of the central region. The different behavior is probably due to the different intensity of turbulent eddies which are generated at the reattachment point downstream the ribs, i.e., the so-called "tumble vortices". In both pictures 5a and 5b, the maximum Nu oscillation

with respect to the average value is around 30%. Therefore, both the absolute and the percentage streamwise variations of the local Nusselt number are significantly lower than the corresponding spanwise variations, depicted in figure 4, and for this reason the trend along the axial direction is not considered appreciable.

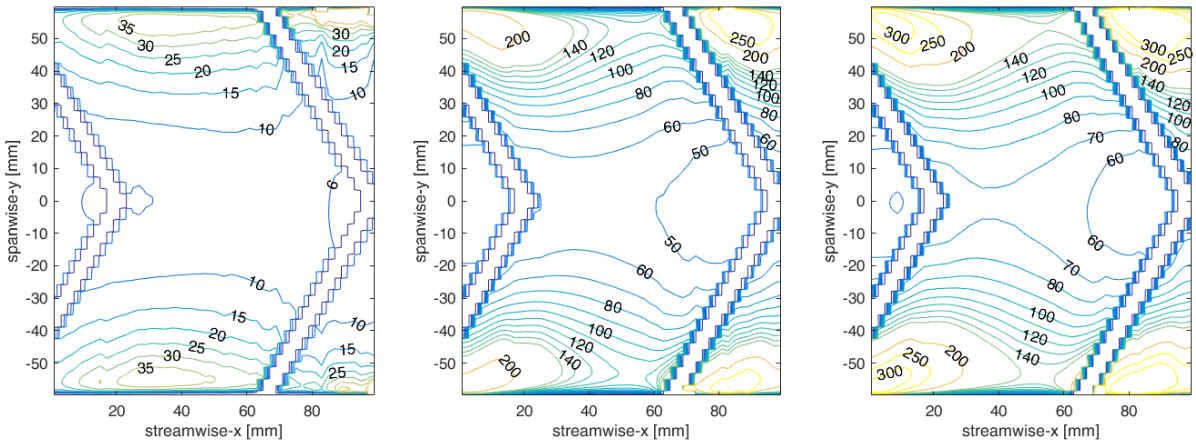

Figure 3. Local Nu contour maps, Re=700 (a), Re=5400 (b) and Re=7550 (c)

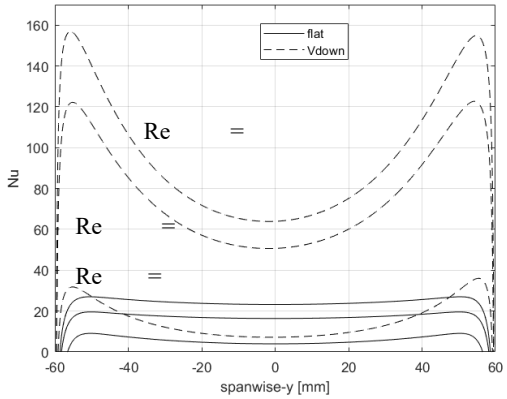

Figure 4. Spanwise Nusselt distribution, x = 40 mm, with flat channel as reference (continuous lines)

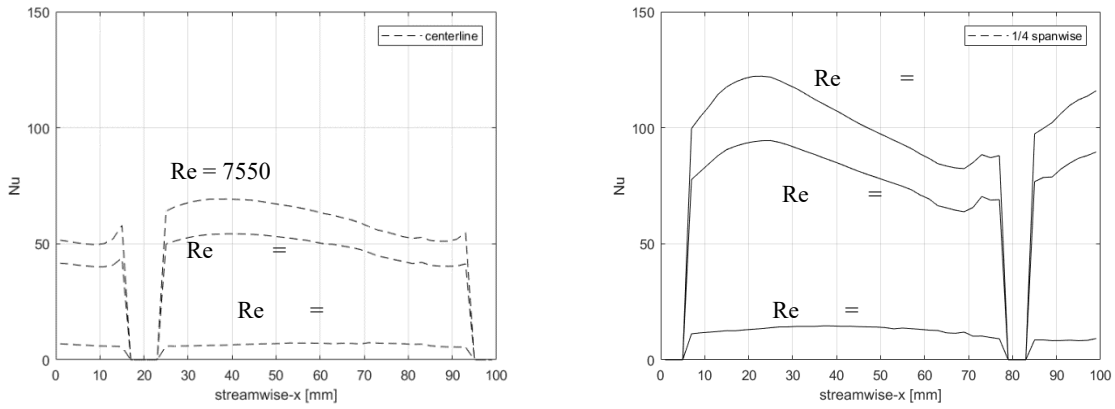

Figure 5. Streamwise Nusselt distribution, centerline (a) and at y = 15 mm (b)

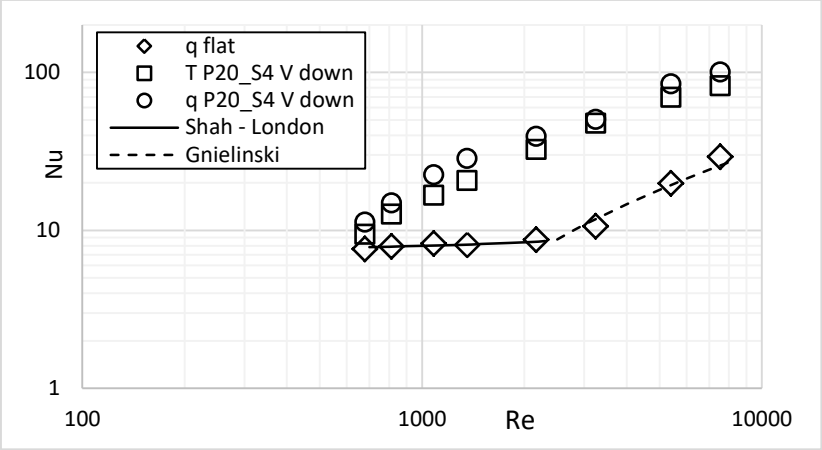

Figure 6. Average Nu on the reference flat channel (q flat, diamonds), compared with global Nu number on a channel with imposed temperature and the same V-down rib configuration (T P20_S4) and with the rib-to-rib average of Nu distribution presented in figure 3 (q P20_S4), for 8 Re. Reference correlations for laminar and turbulent flows in a flat channel are also shown as reference.

Figure 6 presents a comparison of average Nusselt numbers. The average values obtained with the method described in this paper on a flat channel, i.e. without ribs, are shown to fit well the well-known correlations by Shah and London for the laminar regime and by Gnielinski for the post-transitional regime. Moreover, the average rib-to-rib Nusselt number evaluated in this experimental campaign are compared to previous results obtained by the authors on a channel with imposed temperature and the same rib configuration, where a global Nusselt number has been measured, as described in [3]. The averaged local measurements show higher Nu values than the global ones by an average factor of 1.23. This discrepancy should be further investigated, but is probably caused by the influence of the entry region, an example of which can be appreciated on similar ducts on [9].

4 Conclusions

The present study shows the application of the developed technique for the local convective heat transfer estimation with V-shaped ribs. In particular, after a deep assessment phase described in previous works, the local trends seem superior to all the estimated sources of uncertainty, especially towards the lateral edges, were the convective heat flux ceases to be the predominant term in the energy balance. The results seem coherent with previous work in literature, and expand the limits of the analysis to the whole channel. More work is required to model the influence of the ribs, while ongoing DNS studies and flow visualization analyses are carried out to reach definitive answers on this topic.

References

[1] D Fustinoni, P Gramazio, L Vitali and A Niro 2017 *J. of Phys.: Conf. Series* **796** 012015
[2] P Gramazio, L Vitali, D Fustinoni and A Niro 2017 *J. of Phys.: Conf. Series* **923** 012052
[3] P Gramazio, L Vitali, D Fustinoni and A Niro 2018 *proc. of 16th IHTC, Beijing (China) august 10-15,* in press
[4] Han J C, Zhang Y M and Lee C P 1991 *J. Heat Trans.* **113** 590-596
[5] Kukreja R T, Lau S C and McMillin R D 1993 *Int. J. Heat Mass Tran*. **36** 2013-20
[6] Gao X and Sunden B 2001 *Exp. Therm. Fluid Sci.* **24** 25-34
[7] Han J C and Park J S 1988 *Int. J. Heat and Mass Trans.* **31** 183-195
[8] Siegel, R., "Net Radiation Method for Enclosure Systems Involving Partially Transparent Walls" NASA technical note D-7384 (1973). Technical note

[9] Peng W, Jiang P X, Wang Y P, Wei B Y 2011 *App. Therm. Eng.* **31** 2702-2708